IJE TRANSACTIONS B: Applications Vol. 39, No. 11, (November 2026) 2659-2675

International Journal of Engineering

Journal Homepage: www.ije.ir

Increasing the Switching Resource of Circuit Breakers Using a Counter Electromagnetic Field

V. Y. Frolov, V. V. Barskov, D. V. Ivanov*, A. Sabbaghan

Peter the Great St. Petersburg Polytechnic University, Saint Petersburg, Russia

P A P E R I N F O

Paper history:
Received 29 September 2025
Received in revised form 05 February 2026
Accepted 13 February 2026

Keywords:
Switching Resource
High-current Generator Circuits
Electric Arc Quenching
Current Limitation
Counter Electromagnetic Field

A B S T R A C T

Based on the analysis of the switching resource of generator circuit-breakers, the need for current limitation in the generator network was established due to the impossibility of increasing the breaking capacity of the electrical apparatus by traditional methods. An analysis of existing methods of current limitation was given and a new principle of action on a high-current electric arc by a counter electromagnetic field was proposed. The results of experimental studies conducted on a model test bench are presented, along with the outcomes of mathematical modelling of the processes under consideration. A comparison of these results demonstrated good agreement, indicating successful validation of the developed model.Technical solutions for controlling current limitations have been developed. The principle of electromagnetic influence on the arc has been examined in detail, with the determination of the parameters and characteristics of control. A case study performed in the MATLAB Simulink software is presented demonstrating the implementation of the proposed method for limiting short-circuit current in a generator network model. The results illustrate the possibility to limit the short-circuit current to levels at which the generator circuit breaker can successfully perform the interruption.

***doi**: 10.5829/ije.2026.39.11b.02*

Graphical Abstract

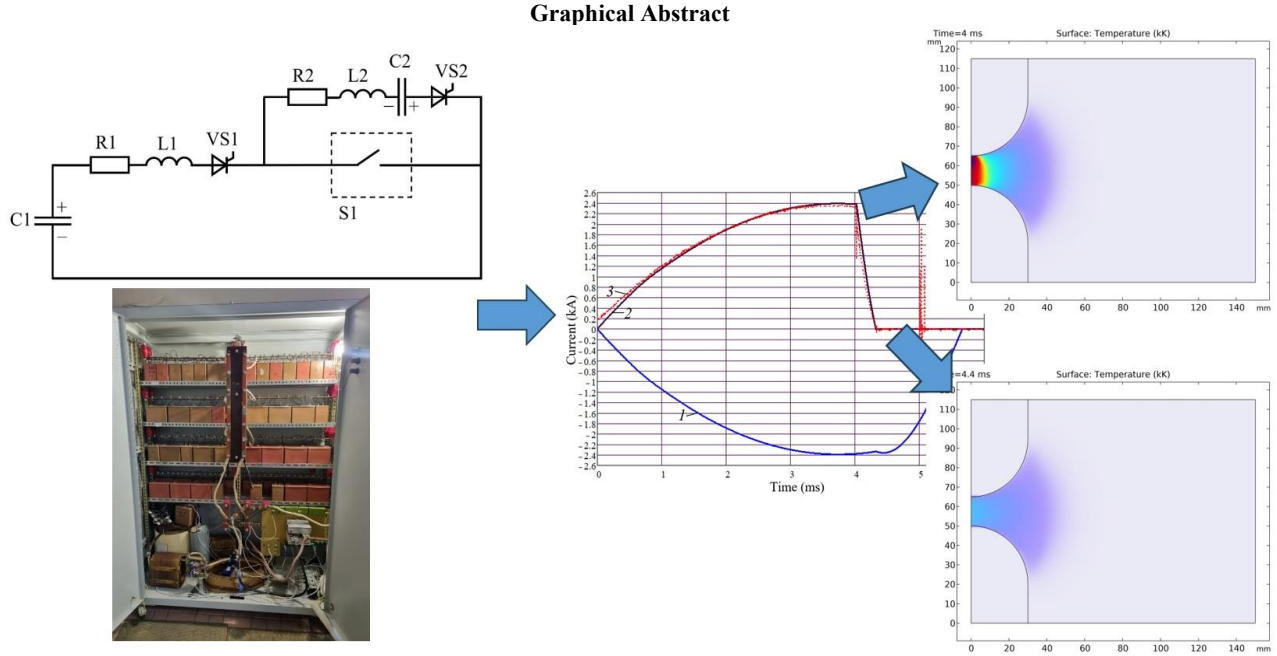

*Corresponding Author Email: d.ivanov@spbstu.ru (D. V. Ivanov)

Please cite this article as: Frolov VY, Barskov VV, Ivanov, DV, Sabbaghan A. Increasing the Switching Resource of Circuit Breakers Using a Counter Electromagnetic Field. International Journal of Engineering, Transactions B: Applications. 2026;39(11):2659-75.

NOMENCLATURE

$C1$, $C2$	capacitances of capacitors	R_{d1}, R_{d2}	resistive voltage divider
$L1$, $L2$	inductances of coils	R_{arc}	arc resistance
I	current	$S1$	circuit breaker under test
$I_{A,max}$, $I_{B,max}$, $I_{C,max}$	maximum phase short-circuit currents	$S2$	switch
I_{arc}	arc current	t	time
$I_{arc,max}$	maximal value of arc current	t_{quench}	arc quenching time
$I_{arc,min}$	minimal value of arc current	U_{arc}	arc voltage
I_{C1}, I_{C2}	current through capacitors C1, C2	U_{ch}	charging voltage
n	number of interruptions	U_{C1}, U_{C2}	voltages on capacitors C1, C2
P_{loss}	arc power loss	U_{L1}, U_{L2}	voltages on inductances L1, L2
Q_0	arc time constant	U_{S1}	voltage on the circuit breaker
$R1$, $R2$	active resistances of coils	VM	voltage multiplier
R_{sh1}, R_{sh2}	shunt resistors	$VS1$, $VS2$	thyristors

1. INTRODUCTION

Increasing the switching resource of circuit breakers is a critical challenge for the modern power engineering industry (1-5).

Analysis of switching devices operation in high-current generator circuits with a power of up to 1200 MW and short-circuit currents of up to 300 kA has shown that modern generator circuit breakers from leading manufacturers such as ABB[1], Siemens[2] and others fail to meet the required switching resource for operation in these networks. The results presented by ABB Company (6) indicate limited resource when operating at rated current (see Table 1). In addition, the HEC-7C (or HEC-10C) generator circuit breaker can interrupt a breaking current of 210 kA only three times over its entire service life.

Recent research and development efforts by leading companies aimed at creating generator circuit breakers that use SF_6 gas for arc quenching (7, 8) have not yielded the expected results due to challenges in dissipating the large amount of energy stored in the electric arc, as well as material durability limitations. Similarly, attempts to increase the breaking capacity using various current-limiting techniques, such as current-limiting reactors (9, 10), have also proven unsuccessful due to stringent requirements for electrodynamic and thermal withstand capabilities.

The following methods for enhancing the switching resource of electrical apparatus are considered promising:

- PTC-thermistor-based current limiting in the circuit breaker's commutation circuit (11-13);
- switching with a hybrid circuit breaker (14, 15);
- the chopper-based current limiting principle (16, 17).

This paper investigates a novel approach to enhancing the switching resource of circuit breakers by acting upon the electric arc with a counter electromagnetic field (see Figure 1). The proposed method demonstrated effective performance in the study, showing promise for practical applications.

Currently, the principle of forced commutation is successfully implemented in apparatuses with semiconductor devices (18-22). This allows for the forced creation of a current zero-crossing, thereby enabling thyristor turn-off. The same principle can be effectively applied to create a counter-current in an electric arc that appeared in switching device, thus ensuring its quenching. In this case, the counter

TABLE 1. Switching resource of the HEC-7C (HEC-10C) generator circuit breaker: number of interruptions (n) as a function of breaking current (I) (6)

I, kA	10	20	30	40	50	60
n	280	65	32	19	15	13

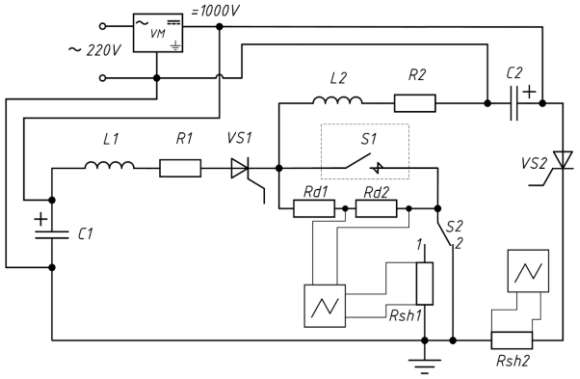

Figure 1. Schematic diagram of the test bench: $S1$ – circuit breaker under test, with a breaking current of 16 kA; $VS1$, $VS2$ – thyristors; $C1$=11.4 mF; $C2$=0.78 mF; $L1$=735 μH; $R1$=0.119 Ω; $L2$=110 μH; $R2$=0.021 Ω; R_{sh1}= R_{sh2}=1.5 mΩ (parameter values were measured using a TESLA BM 591 RLC meter at a frequency of 100 Hz). In the schematic: VM – voltage multiplier; R_{sh1}, R_{sh2} – shunt resistors; R_{d1}, R_{d2} – resistive voltage divider; $S2$ – switch (position 1 – for measuring the current through circuit breaker $S1$ via R_{sh1}, position 2 – for measuring the voltage across circuit breaker $S1$ via the R_{d1}, R_{d2} voltage divider)

[1] https://global.abb/
[2] https://www.siemens.com

electromagnetic field generated by the discharge of a capacitor bank forces the arc current to decrease. Two scenarios are then possible:

1. The current is reduced to zero, ensuring deionization of the contact gap and recovery of the dielectric strength.

2. The current is reduced to a level at which the arc can be readily quenched by the given switching device.

The application of a counter electromagnetic field to the electric arc was previously studied in the context of DC networks, where it enabled an increase in the breaking capacity of DC circuit breakers (23-25).

In this paper, we propose applying this arc-control method to AC generator networks with switching currents exceeding 200 kA.

Due to the complexity of conducting experimental studies in actual generator networks, it was decided to carry out both experimental and theoretical investigations using a model. Then the proposed method of influencing the electric arc will be transferred to high-current generator networks.

The physical model under consideration was a magnetic blast circuit breaker with breaking current 16 kA ($S1$ in Figure 1). The study focused on forced arc quenching (according to the electric scheme in Figure 1) under the influence of a counter electromagnetic field controlled by the time moment of the counter-current injection via thyristors.

2. MATERIALS AND METHODS

2. 1. Experimental Investigations of Electric Arc Quenching by a Counter Electromagnetic Field

To establish the patterns of electric arc quenching and to evaluate the feasibility of the proposed method of controlled current limitation through the dissipation of electromagnetic energy by a counter electromagnetic field, the investigation was initially performed experimentally. For this purpose, a test bench was assembled. The general view of the test bench and the contacts of the circuit breaker under investigation are shown in Figure 2.

A measurement system was set up to perform precise measurements of the switching process parameters and arc-quenching characteristics. This system was based on the following instruments:

1. Two AKIP-4115/1A oscilloscopes.

2. Three FNIRSI P6100 voltage probes (1:1 / 1:10, 100 MHz).

3. Two 75ShIP1-50-0.5 current shunts.

4. Two UT58C (13-1023) digital multimeters.

Metrological characteristics of the measurement system:

1. Arc voltage, measured by an oscilloscope via a 1:10 voltage divider. Range: 0–600 V.

2. Arc current, measured using a 75ShIP1-50-0.5 current shunt and recorded by an oscilloscope via a 1:1 divider.

3. Counter LC-circuit current, measured using a 75ShIP1-50-0.5 current shunt and recorded by an oscilloscope via a 1:1 divider.

4. Voltage across the capacitors, monitored by a UT58C digital multimeter.

The following operational procedure was employed during the measurements (see Figure 1):

1. The capacitor banks $C1$ and $C2$ were pre-charged to an identical initial voltage U_{ch}.

2. Thyristor $VS1$ is triggered, enabling capacitor $C1$ to discharge through circuit breaker $S1$, initiating and sustaining an electric arc across its contacts.

3. After an adjustable time delay (set to 4 ms in the experiments), thyristor $VS2$ is triggered. This causes capacitor $C2$ to discharge, generating a counter-current through circuit breaker $S1$.

2. 2. Mathematical Modeling of Electric Arc Quenching by a Counter Electromagnetic Field

To investigate the dissipation of electromagnetic energy by a counter electromagnetic field generated by high-power semiconductor devices, a mathematical model was

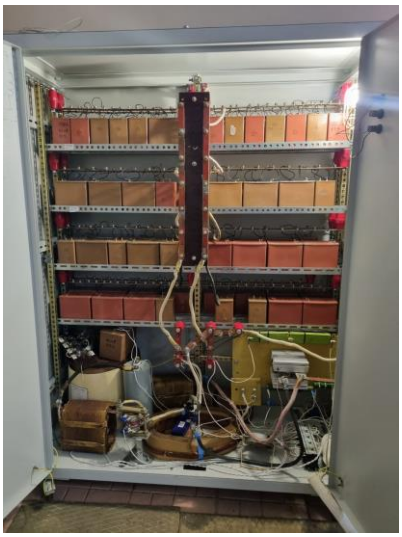

(a)

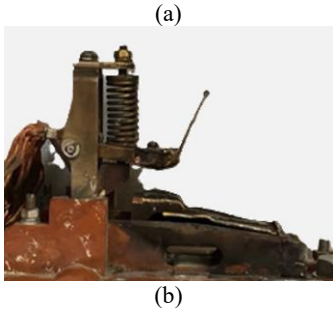

(b)

Figure 2. Experimental test bench: (a) general view; (b) circuit breaker contacts

developed. This model describes the thermal, gas-dynamic, and electromagnetic processes in the electric arc, coupled with the processes in the electrical circuit.

The main equations of the applied model for plasma processes express fundamental conservation laws (26):

- energy equation;
- momentum equation;
- continuity equation.

Since plasma exists within an electromagnetic field, the system of equations is supplemented by Maxwell's electromagnetic equations. These are reduced to equations for the scalar electric and vector magnetic potentials.

The thermodynamic and transport properties of air plasma as functions of temperature at a pressure of 1 atm were pre-calculated using the methodology described by Dresvin et al. (27). The dependence of plasma density on pressure was accounted for by employing the ideal gas equation of state.

Due to the short duration of the processes in the discharge chamber, radiation is the significant mechanism of arc energy transfer. This process was taken into account using the approach proposed by Mürmann et al. (28), which has proven to be reliable in previous studies (29).

The system of equations described above was solved using the finite element method with the COMSOL Multiphysics software.

The geometry of the computational domain is shown in Figure 3. The domain consists of two rounded copper electrodes with a diameter of 60 mm, spaced 15 mm apart. They are surrounded by a cylindrical air region with a diameter of 300 mm and a height of 115 mm. Splitter plates of the arc extinguishing chamber is located outside the computational domain.

The boundary conditions for this task are defined based on fundamental physical considerations:

- A temperature of 293 K is prescribed on the external boundaries of the electrodes and on the radial boundary of the computational domain, due to their remoteness from the arc region;

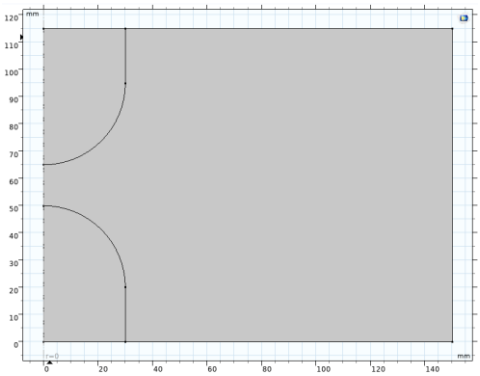

Figure 3. Computational domain

- A thermal insulation condition is applied on the remaining boundaries for the temperature field, specifying a zero heat flux;
- For the gas dynamics problem, a zero gauge pressure condition is set at the open boundaries;
- For the electromagnetic problem, the external boundary of one electrode is grounded (zero electric potential is specified for computational convenience and result presentation). A Terminal boundary condition is applied to the external boundary of the other electrode to couple the model with the external circuit.

A temperature of 293 K, zero velocity, and zero gauge pressure was set as the initial conditions for the computational domain.

The external electrical circuit was modeled using the Electrical Circuit module. A model of the circuit, shown in Figure 1, was implemented within this module.

3. RESULTS AND DISCUSSION

3. 1. Results of Experimental Investigation The measured current and voltage oscillograms are presented in Figures 4 and 5.

Figure 4 shows the measurement results for two arc quenching scenarios:

- Case 1 (charging voltage $U_{ch,1}$=500 V): the oscillograms of the arc current and of the voltage on the circuit breaker (Figure 4a) as well as the oscillogram of the counter-current, i.e., the discharge current of capacitor $C2$ (Figure 4b);
- Case 2 (charging voltage $U_{ch,2}$=900 V): the oscillograms of the arc current and of the voltage on the circuit breaker (Figure 4c) as well as the oscillogram of the counter-current, i.e., the discharge current of capacitor $C2$ (Figure 4d).

Since the obtained oscillograms for the two cases are similar, we will analyze in detail the ones for the maximum investigated charging voltage of U_{ch}=900 V (Figure 4, c, d).

It can be observed that when thyristor $VS1$ is switched on and the contacts of the circuit breaker $S1$ open, the arc current rises to a value of 2.3 kA. Subsequently, upon the triggering of thyristor $VS2$ and the injection of the counter-current, the arc current decreases to zero within 0.3 ms, indicating successful circuit breaker arc quenching.

Prior to the activation of thyristor $VS2$, the counter-current (the discharge current of capacitor $C2$) was zero. After triggering, it rapidly increases to a peak of 2.3 kA and then, after arc quenching, it decays to zero due to the recharging of capacitor $C2$.

Analysis of the voltage oscillograms reveals several distinct phases of the process.

During the initial period, an uneven increase in voltage is observed, accompanied by characteristic

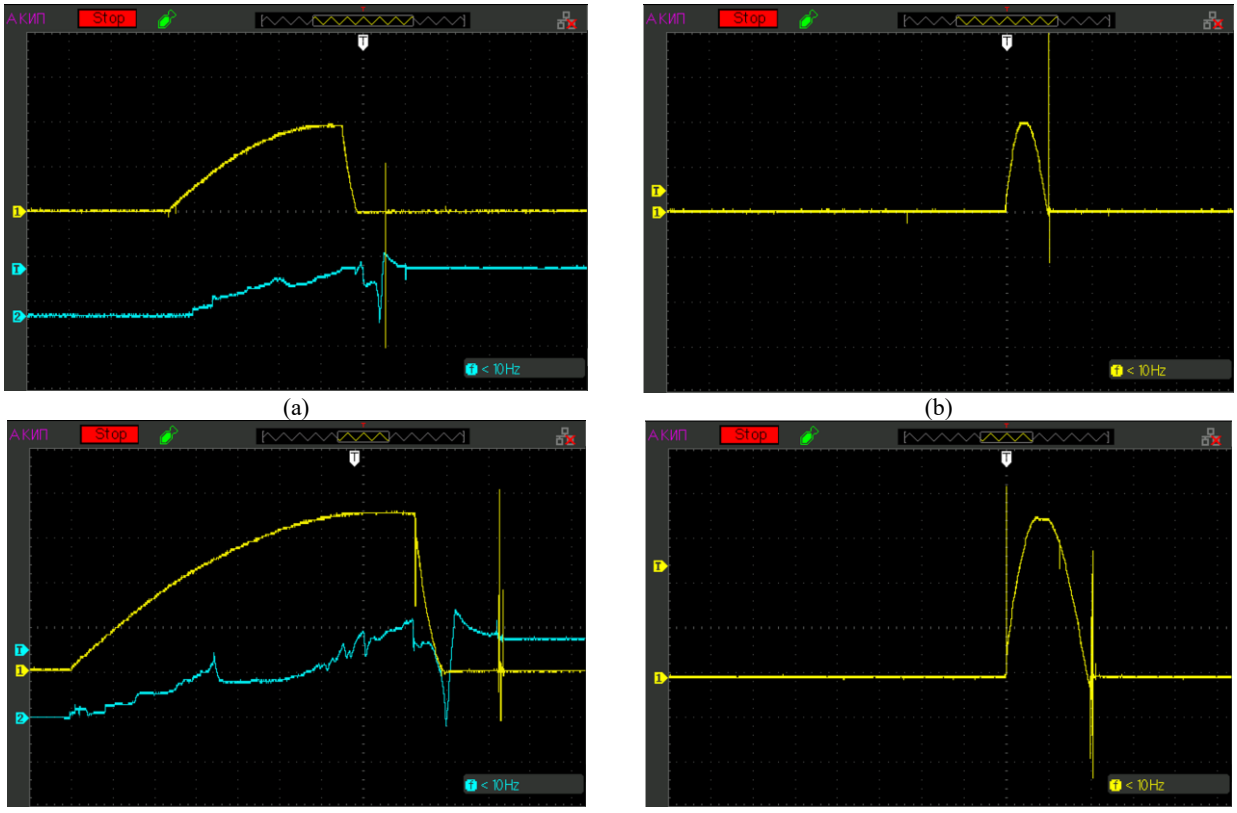

(a) (b)

(c) (d)

Figure 4. Measurement results for cases with arc quenching: (a) Arc current (yellow curve) and voltage on the circuit breaker (turquoise curve) at U_{ch}=500 V (m_I=667 A/div, m_U=100 V/div, m_t=1 ms/div); (b) Counter-current (discharge current of capacitor $C2$) at U_{ch}=500 V (m_I=667 A/div, m_t=1 ms/div); (c) Arc current (yellow curve) and voltage on the circuit breaker (turquoise curve) at U_{ch}=900 V (m_I=667 A/div, m_U=100 V/div, m_t=0.5 ms/div); (d) Counter-current (discharge current of capacitor $C2$) at U_{ch}=900 V (m_I=667 A/div, m_t=0.5 ms/div)

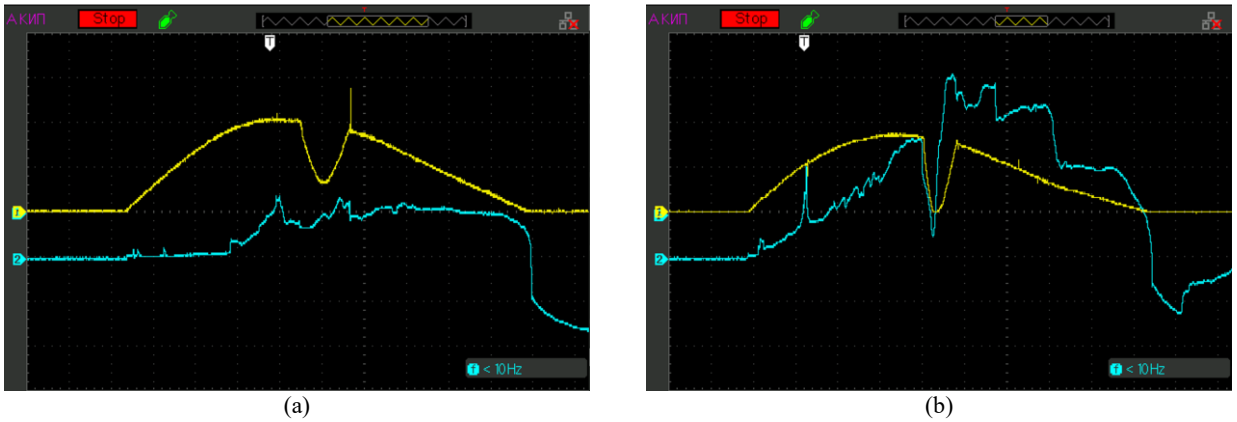

(a) (b)

Figure 5. Measurement results for cases without arc quenching: (a) Arc current (yellow curve) and voltage on the circuit breaker (turquoise curve) at U_{ch}=500 V (m_I=667 A/div, m_U=100 V/divm, m_t=1 ms/div); (b) Arc current (yellow curve) and voltage on the circuit breaker (turquoise curve) at U_{ch}=900 V (m_I=1333 A/div, m_U=100 V/div, m_t=1 ms/div)

amplitude oscillations, which is a clear indication of arc discharge development. A voltage dip of approximately 40 V is particularly indicative, that is alternating with a region of relative stabilization. This behavior provides evidence of the complex physical processes occurring within the arc plasma channel. The maximum recorded voltage reaches 211 V, reflecting the peak intensity of the arcing process at the maximum arc current.

Following the injection of the counter-current and the beginning of the arc current decay, the graph

demonstrates an abrupt change in the process character – the arc voltage drops sharply to a level of 150 V and maintains this value throughout the entire quenching time of 0.318 ms. Such a stable voltage level during the quenching phase indicates the establishment of an equilibrium state between the supplied energy and the process of deionization in the arc gap under the influence of the counter-current.

Of particular note is the complex transient process observed after the complete quenching of the arc (Figure 4c). Once the arc current reaches zero, the voltage continues to decrease towards zero. However, 0.284 ms after arc extinction, a voltage surge to 240 V occurs, followed by a gradual decline to 170 V. This effect can be explained by energy redistribution processes within the system. After the final arc quenching, the measurement system ceases to record the voltage drop across the arc itself (which has already ceased to exist) and instead begins to measure the potential difference between two points in the circuit. These points are connected by a common loop that includes capacitive elements. In this context, the observed voltage surge can be attributed to the redistribution of energy between the system components: primarily, the loop inductance and capacitive storage elements. It is particularly important to note that the steady, constant voltage established after the complete ending of all transient processes represents the residual voltage on the capacitor. This residual voltage is caused by the incomplete dissipation of the stored energy during the quenching process.

To demonstrate the controllability of this arc quenching method, experiments were conducted on the test bench in which the arc was not extinguished due to varying the circuit parameters. Two cases were considered, with the following modifications to the parameters of the second circuit (see Figure 1):

- Case 3: $C2 = 0.56$ mF, $R2 = 0.3$ Ω;
- Case 4: $C2 = 0.56$ mF.

The charging voltage for Case 3 was $U_{ch,3} = 500$ V, and for Case 4 – $U_{ch,4} = 900$ V.

Figure 5 shows the oscillograms of the arc current and arc voltage for the cases without arc extinction. These oscillograms demonstrate that upon the injection of the counter-current, the arc current (yellow curve) decreases. However, the energy stored in the capacitor is insufficient to force the current through zero and quench the arc. Consequently, after the counter-current pulse subsides, the arc reignites and continues to burn.

3. 2. Results of Mathematical Simulation

Subsequently, for a detailed analysis of the occurring processes, mathematical simulation of all performed experimental cases was carried out, along with a comparison of the simulation results with the experimental data.

Calculations using the developed model were performed in three stages.

During the first stage, lasting 4 ms, thyristor $VS1$ is open and thyristor $VS2$ is closed. Capacitor $C1$ discharges through the electric arc, leading to its development and expansion.

During the second stage, lasting 1–2 ms (depending on the specific case), thyristor $VS2$ is opened, and capacitor $C2$ discharges. As a result, a counter-current passes through the electric arc.

During the third stage (only for the cases with successful arc extinction), which lasts no more than 10 ms, the model of thermal, gas-dynamic, and electromagnetic processes is excluded from the calculation to accelerate computations. Only the processes occurring in the electrical circuit are simulated.

The simulation results are presented in Figures 6-11. The time dependencies show a period of up to 6 ms, as by this time:

- in cases with successful arc extinction, the current flow processes in the considered electrical circuit are completed;
- in cases without arc extinction, capacitor $C2$ is fully discharged.

Furthermore, the time dependencies of currents and voltages provide a more detailed view of the time interval during which the counter-current is applied (the time interval of 3.9–4.4 ms for cases with successful arc extinction, and 3.9–5.2 ms for cases without extinction).

Let us consider in more detail the processes occurring in the electrical circuit in Case 1 (charging voltage is $U_{ch,1}$=500 V, successful arc extinction). The time dependencies of the currents (see Figure 6, a, b) show that the arc current increases and reaches a steady-state regime during the first stage (the arc development stage), the arc current attains a value of 1280 A and practically ceases to change. Then, at the time instant of 4.01 ms, the thyristor $VS2$ is turned on, the capacitor $C2$ begins to discharge, the current through the arc decreases to zero (at $t = 4.325$ ms), and the arc is extinguished. Thereafter, the current through the capacitors $C1$ and $C2$ continues due to the energy stored in the inductances $L1$ and $L2$ until the recharge of the capacitor $C2$ (since capacitance $C2$ is 14.6 times smaller than capacitance $C1$). The resulting time dependence of the current through the capacitor $C1$ represents the sum of the arc currents and ones through the capacitor $C2$ (to avoid overlapping with arc current on the graph, the current I_{C1} is taken with the opposite sign). Additionally, the experimental values of the arc current are indicated by dots in Figure 6, a, b. A comparison of the calculated and experimental data shows close values of the arc current, with a discrepancy of 5–10%.

The time dependencies of the voltages (Figure 6, c, d) show that the capacitor $C1$ discharges from the initial charging voltage of 500 V to a voltage of 186 V by the

time instant of 4 ms. Meanwhile, the voltage on the capacitor $C2$ remains unchanged (since the thyristor $VS2$ is off) and is equal to –500 V. The voltage on the circuit breaker increases during the time interval of 0–1 ms and then remains practically constant (144–146 V).

The voltage on the inductance $L1$ at the initial time instant is equal to the voltage on the capacitor $C1$ and determines the rate of rise of the arc current. Then, as the current increases, the voltage on the inductance $L1$ decreases to zero (at t = 3.81 ms) and subsequently becomes negative (–21 V at t = 4 ms) due to a slight decrease in the current during this time interval.

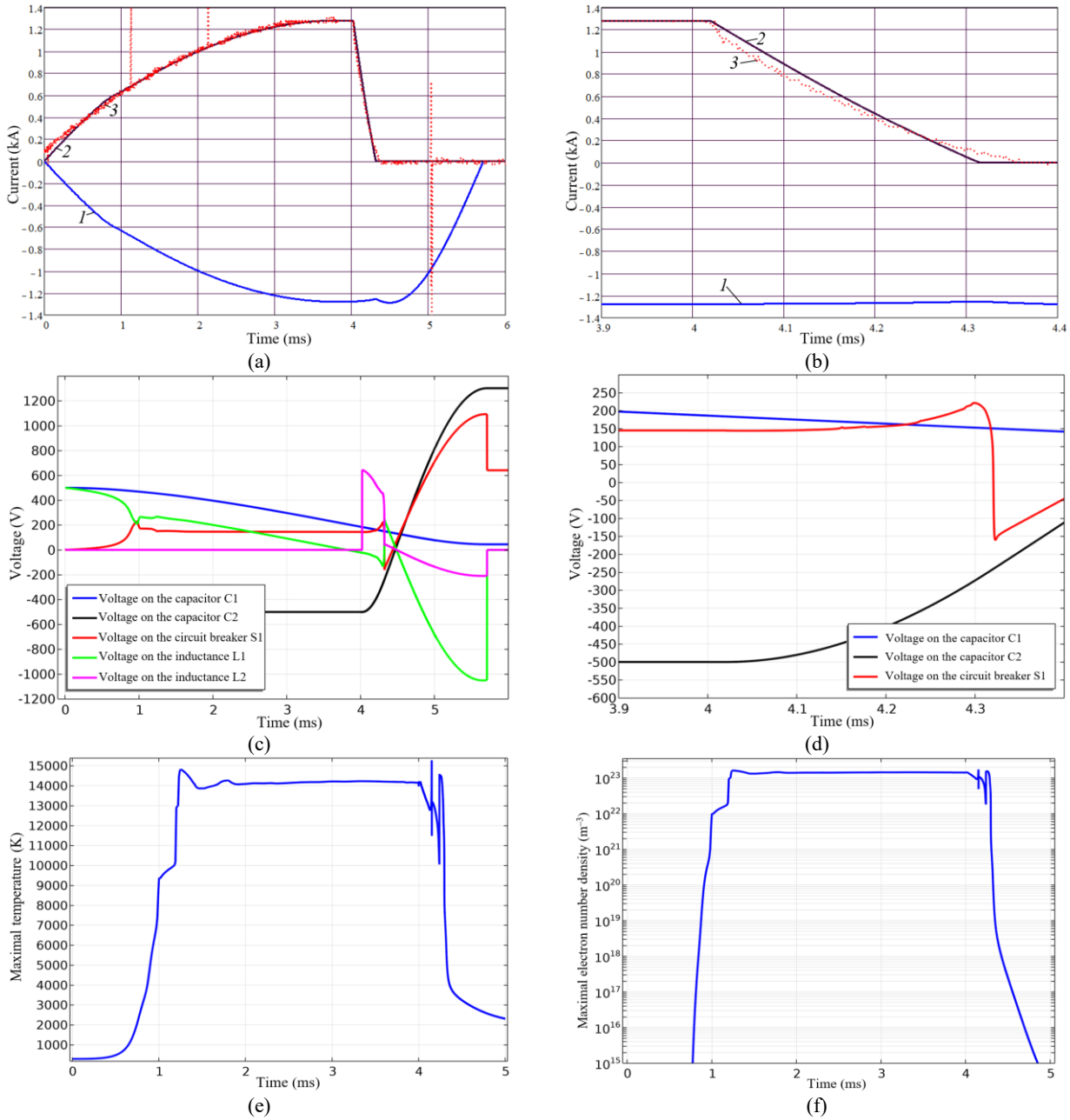

Figure 6. Calculated time dependencies of parameters for the case with successful arc extinction, charging voltage is $U_{ch,1}$ = 500 V (Case 1): a, b – currents in the circuit under consideration (a – for the time interval of 0-6 ms; b – for the time interval of 3.9-4.4 ms; 1 – current through capacitor $C1$; 2 – arc current; 3 – arc current, experiment); c, d – voltages in the circuit under consideration (c– for the time interval of 0-6 ms; d – for the time interval of 3.9-4.4 ms); e – maximum plasma temperature; f – maximum electron number density

Then, at the time instant of 4.01 ms, the thyristor *VS*2 is turned on, and the capacitor *C*2 begins to discharge. For this time interval, according to Kirchhoff's voltage law, the following equation can be written:

$$U_{L2} = U_{arc} - U_{C2}. \quad (1)$$

Therefore, a significant voltage (645 V) is applied to the inductance *L*2 when the thyristor *VS*2 is turned on. This voltage then decreases as the capacitor *C*2 discharges. By the time instant of 4.3 ms, the capacitor *C*2 discharges from –500 V to –273 V.

At the time instant of 4.3 ms, the arc voltage (the voltage on the circuit breaker) reaches its maximum value of 221 V, after which the arc is extinguished and the arc current drops to zero. Simultaneously, the current I_{C2} increases to match I_{C1}, resulting in $I_{C2} = I_{C1}$. This leads to a sharp decrease in the rate of change of I_{C2}, causing a rapid drop in the voltage U_{L2} (from 443 V to 37 V at $t = 4.325$ ms). Since the voltage on the interelectrode gap of the circuit breaker *S*1 (it is incorrect to refer to this one as arc voltage after arc extinction)

$$U_{S1} = U_{L2} + U_{C2}, \quad (2)$$

and the voltage U_{L2} decreases sharply, U_{S1} also decreases (from 221 V to –159 V).

Furthermore, according to Kirchhoff's voltage law:

$$U_{L1} = U_{C1} - U_{S1}, \quad (3)$$

and the voltage U_{S1} decreases sharply, it leads to a sharp increase in U_{L1} (from –129 V to 243 V at $t = 4.325$ ms).

Subsequently, the capacitors continue to discharge along the circuit *C*1-*L*1-*R*1-*VS*1-*L*2-*R*2-*C*2-*VS*2-*C*1 (see Figure 1). Here, the current I_{C1}=I_{C2} reaches its maximum at $t = 4.48$ ms (where $U_{L1} = U_{L2} = 0$), and then begins to decrease (causing U_{L1} and U_{L2} to become negative).

The subsequent transient process in the electrical circuit evolves according to the energy stored in the capacitors and inductances at the moment of arc extinction. Since the capacitance of the capacitor *C*2 is 14.6 times smaller than that of the capacitor *C*1, it becomes recharged to a voltage of 1302 V. Meanwhile, the voltage across capacitor *C*1 at the end of the transient process is 45 V. A similar situation is observed in experimental studies.

If there were no thyristors in the electrical scheme, the current would reverse direction after the capacitors were recharged, and a damped oscillatory process would occur in the circuit (since it would represent a series resonant circuit) until the voltages across the capacitors equalized. However, the current cannot flow in the reverse direction due to the presence of the thyristors. Therefore, current ceases to change after it decreases to zero. Consequently, the voltages on the inductances U_{L1} and U_{L2} drop abruptly to zero (*Ldi/dt*), and the voltage on the circuit breaker also decreases abruptly.

Figure 6 e, f shows the time dependencies of plasma parameters obtained using the electric arc model.

Figure 6e shows that the maximum plasma temperature increases during the time interval of 0–1.5 ms (plasma heating occurs) and then practically stabilizes (ranging between 14.1–14.2 thousand K). Then, at the time instant of 4.01 ms, the counter-current from capacitor *C*2 begins to flow, and the arc current starts to decrease. This leads to a sharp decrease in the maximum temperature at a rate of $1.6 \cdot 10^8$ K/s. Notably, the graph (see Figure 6e) also shows local maxima, which can be explained by the reduction in arc diameter, increase in current density, and local overheating of the plasma. By the time instant of 4.325 ms, when the arc current reaches zero, the maximum temperature is 5200 K. Thereafter, the maximum temperature of the hot gas slowly decreases at an average rate of $4.3 \cdot 10^6$ K/s due to convection and thermal conductivity.

The maximum electron number density is shown in Figure 6f. The shape of this dependency largely replicates that of the maximum temperature. It should be noted that the maximum electron number density reaches $1.4 \cdot 10^{23}$ m^{-3} during the arc burning stage, while at the time instant of 4.325 ms when the arc current is zero and arc extinction occurs, the maximum electron number density is $8 \cdot 10^{19}$ m^{-3}.

Figure 7 shows similar dependencies for Case 2 (charging voltage is 900 V, successful arc extinction). The dependencies are largely analogous, differing only in higher currents in the electrical circuit (including the arc current) due to the increase in charging voltage.

Thus, the maximum arc current is $I_{arc,max}$=1283 A for the charging voltage of $U_{ch,1}$=500 V, while it reaches $I_{arc,max}$=2390 A for $U_{ch,2}$=900 V. The increase in arc current leads to a higher energy stored in the electric arc. Nevertheless, despite this increase, arc quenching is still achieved through the dissipation of electromagnetic energy by the counter magnetic field.

Figure 8 shows the plasma temperature distributions at different time instants for Case 2 ($U_{ch,2}$=900 V, successful arc extinction). It can be observed that the temperature and diameter of the arc discharge increase between 0 and 3 ms, reaching their maximum values at approximately 3 ms. Subsequently, the temperature remains relatively constant, as the current remains nearly unchanged during this period (see Figure 7, a). After the injection of the counter-current (in the time interval of 4.1–4.4 ms), the arc current decreases, leading to a rapid reduction in both the arc diameter and its temperature.

Figure 9 shows the simulation results for Case 3 ($U_{ch,3}$=500 V, without arc extinction). The first stage (arc development stage), corresponding to the time interval of 0–4 ms, closely replicates the results obtained for Case 1.

From Figure 9, a, b, it can be observed that the arc current begins to decrease at time moment $t = 4.01$ ms

due to the injection of the counter-current from the capacitor $C2$. However, the energy stored in the capacitor $C2$ is insufficient to quench the arc because of its reduced capacitance (0.56 mF versus 0.78 mF for Cases 1 and 2). The minimum arc current value, $I_{arc,min}$ = 434 A is reached at t = 4.594 ms. Subsequently, the arc current increases to a value of 1114 A at t = 5.1 ms. The original current value (i.e., the arc current at the moment of thyristor $VS2$ triggering) is not reached due to the partial discharge of capacitor $C1$. The simulation was terminated at t = 6 ms. By this time, the voltages on the capacitors were U_{C1} = –49 V and U_{C2} = 766 V (see Figure 9, c).

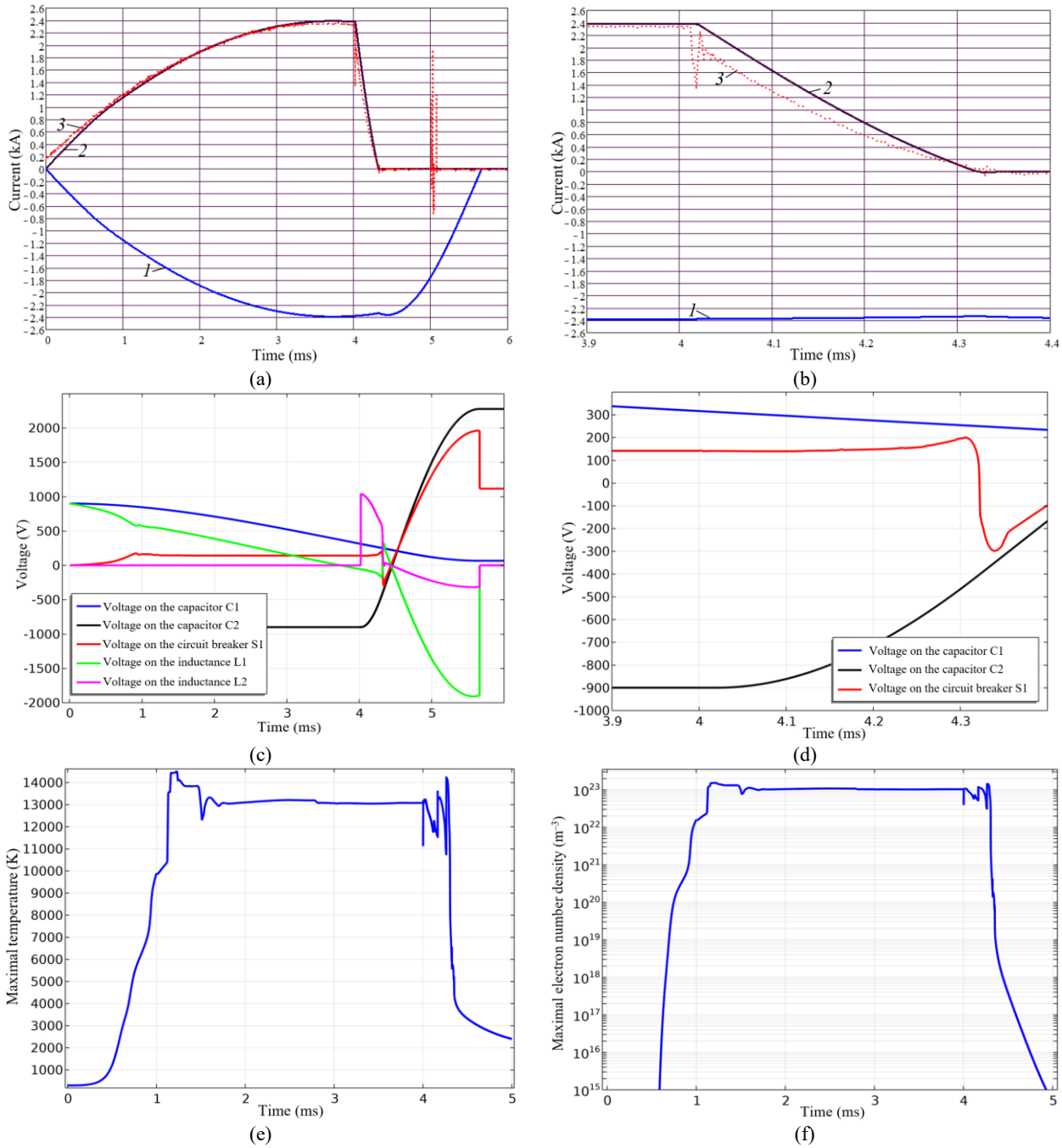

Figure 7. Calculated time dependencies of parameters for the case with successful arc extinction, charging voltage is $U_{ch,2}$ = 900 V (Case 2): a, b – currents in the circuit under consideration (a – for the time interval of 0-6 ms; b – for the time interval of 3.9-4.4 ms; 1 – current through capacitor $C1$; 2 – arc current; 3 – arc current, experiment); c, d – voltages in the circuit under consideration (c– for the time interval of 0-6 ms; d – for the time interval of 3.9-4.4 ms); e – maximum plasma temperature; f – maximum electron number density

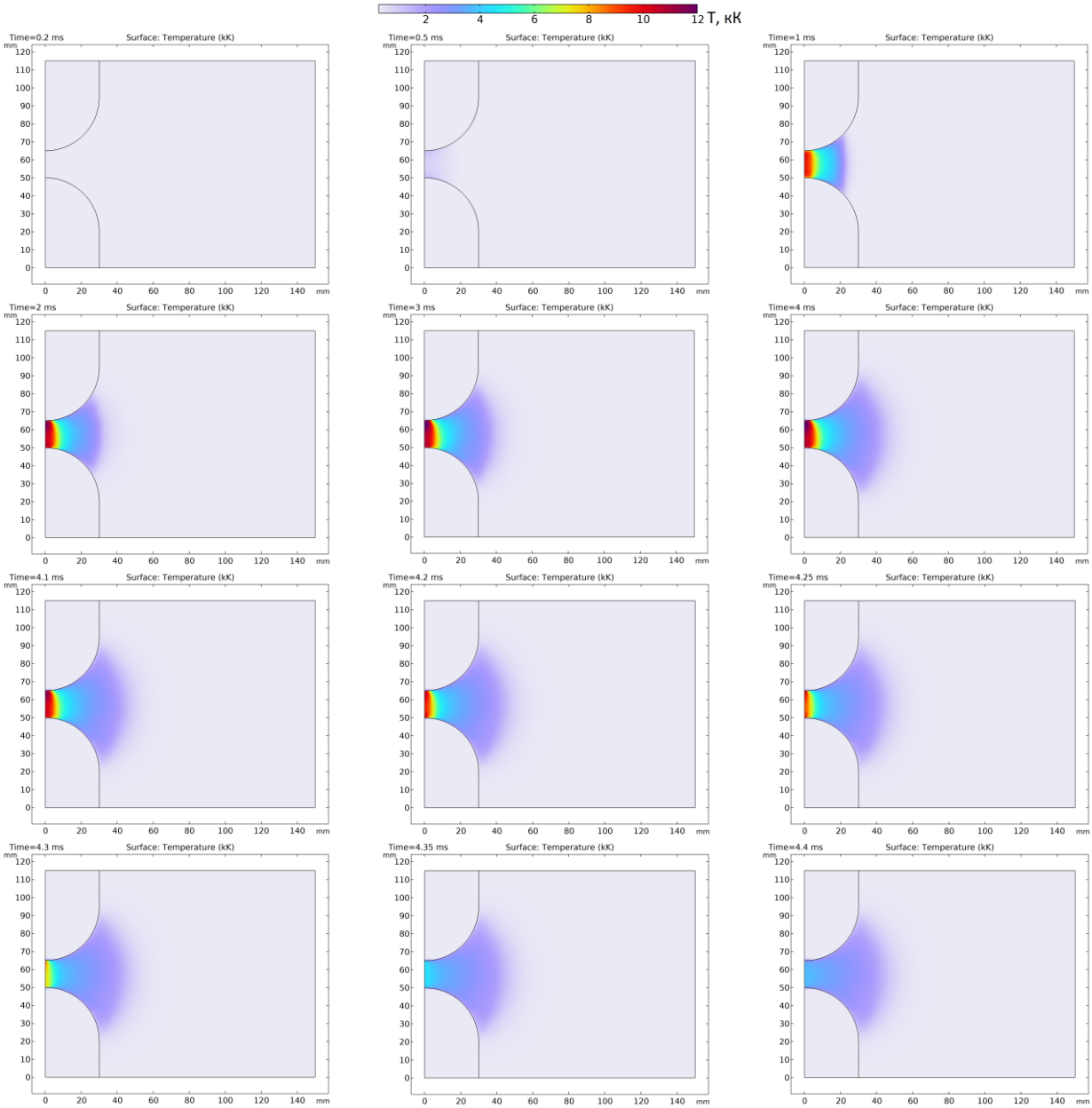

Figure 8. Distribution of arc plasma temperature at different time moments for the case of successful arc extinction, charging voltage is $U_{ch,2}$ = 900 V (Case 2) for the following moments of time (in ms): 0.2; 0.5; 1; 2; 3; 4; 4.1; 4.2; 4.25; 4.3; 4.35; 4.4

Figure 10 shows the simulation results for Case 4 ($U_{ch,4}$=900 V, without arc extinction). The first stage (arc development stage), corresponding to the time interval of 0–4 ms, closely replicates the results obtained for Case 2.

As can be seen from Figure 10, a b, the minimum arc current value of 47 A is reached at t = 4.41 ms. Subsequently, the arc current increases, reaching a value of 2046 A at t = 4.74 ms, indicating that arc quenching did not occur.

Furthermore, as is evident from Figure 10c, d, the arc voltage was equal 141 V at t = 4.01 ms and increased as the arc current decreased. The maximum voltage of 323 V was reached at t = 4.43 ms. Subsequently, as the arc current increased, the arc voltage returned to its previous value of 142 V by t = 5 ms.

The time dependence of the maximum temperature (Figure 10e) shows that as the current gets closer to zero (decreasing from 2390 A to 47 A), the maximum temperature drops to 7038 K at t = 4.41 ms. The maximum electron concentration at this moment decreased to $7 \cdot 10^{20}$ m^{-3} (see Figure 10f). This moment appears to represent a critical threshold for the existence of the electric arc, on the verge of extinction.

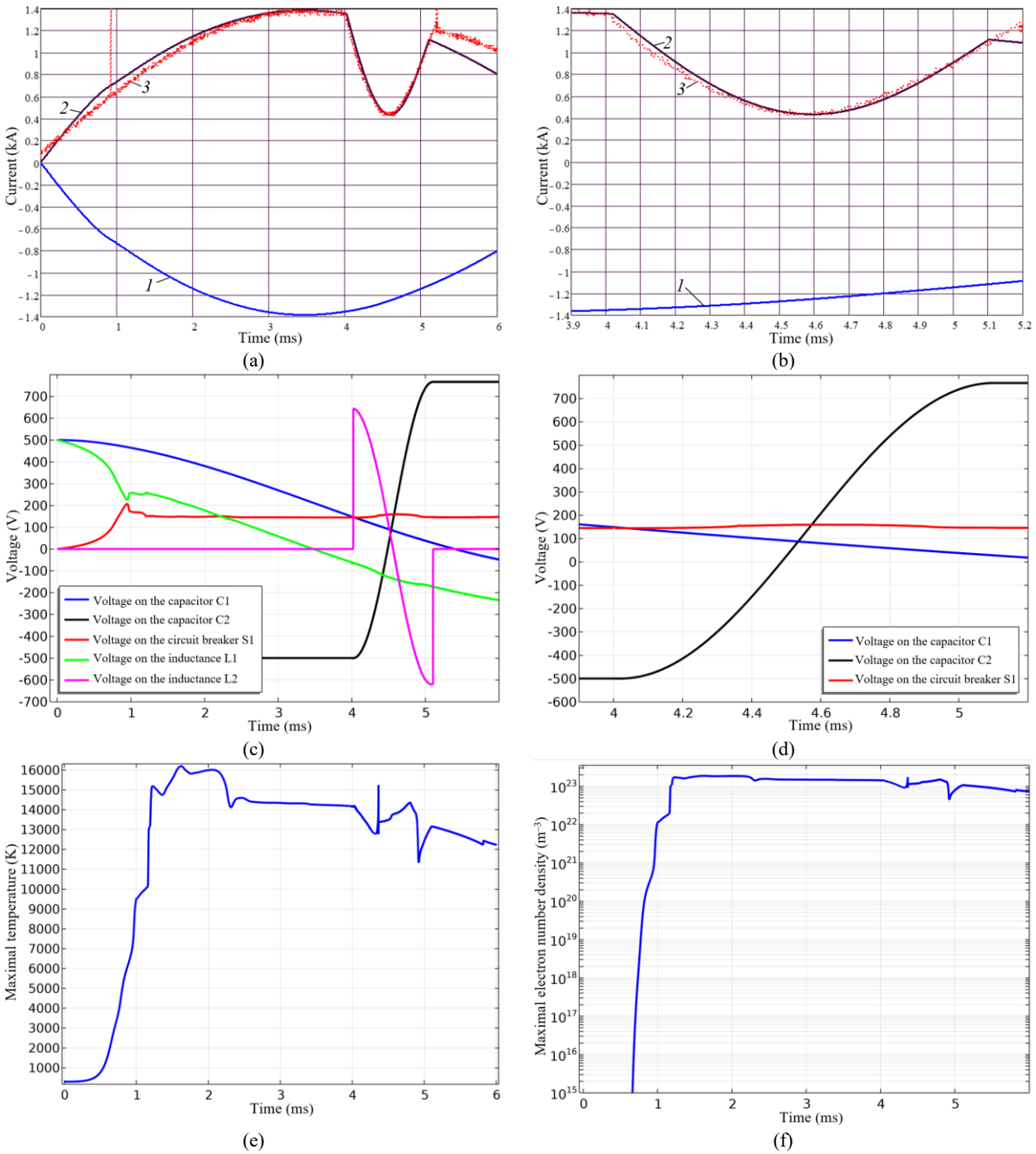

Figure 9. Calculated time dependencies of parameters for the case without arc extinction, charging voltage is $U_{ch,3}$ = 500 V (Case 3): a, b – currents in the circuit under consideration (a – for the time interval of 0-6 ms; b – for the time interval of 3.9-5.2 ms; 1 – current through capacitor *C*1; 2 – arc current; 3 – arc current, experiment); c, d – voltages in the circuit under consideration (c– for the time interval of 0-6 ms; d – for the time interval of 3.9-5.2 ms); e – maximum plasma temperature; f – maximum electron number density

Figure 11 shows the temperature distributions at different time instants for Case 4. The obtained results reveal three distinct stages of arc evolution. The first stage is arc development stage (time interval: 0–4 ms): the interelectrode gap is heated, the arc diameter increases, and a steady-state regime is established. The second one is counter-current rise stage (time interval: 4–4.41 ms): the counter-current leads to a decrease in arc

current, temperature and, therefore, velocity and overpressure. The third one is counter-current decay stage (time interval: 4.41–4.72 ms): the arc current increases again, and the arc discharge recovers nearly to its state at the end of the first stage.

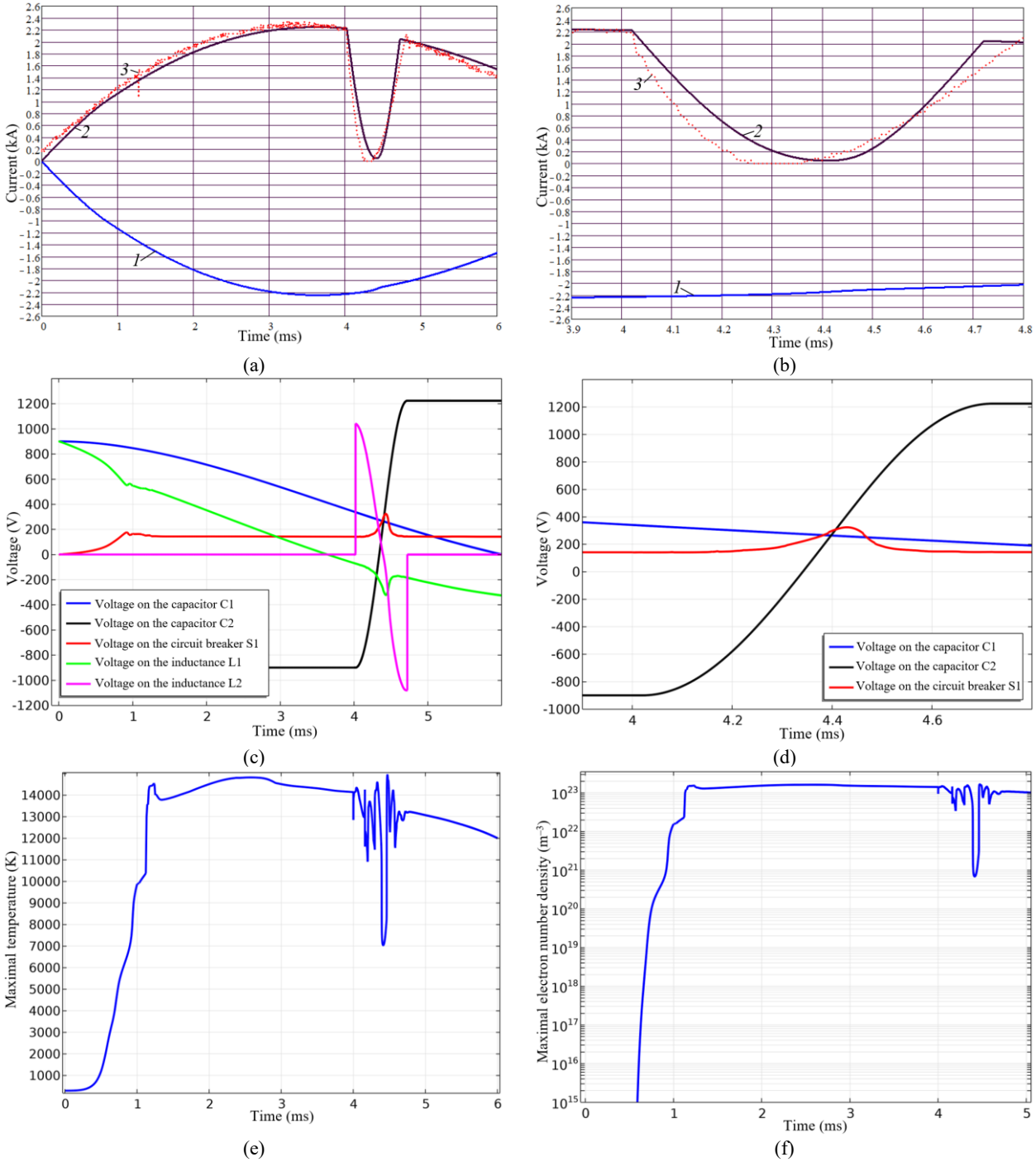

Figure 10. Calculated time dependencies of parameters for the case without arc extinction, charging voltage is $U_{ch,4}$ = 900 V (Case 4): a, b – currents in the circuit under consideration (a – for the time interval of 0-6 ms; b – for the time interval of 3.9-4.8 ms; 1 – current through capacitor $C1$; 2 – arc current; 3 – arc current, experiment); c, d – voltages in the circuit under consideration (c– for the time interval of 0-6 ms; d – for the time interval of 3.9-4.8 ms); e – maximum plasma temperature; f – maximum electron number density

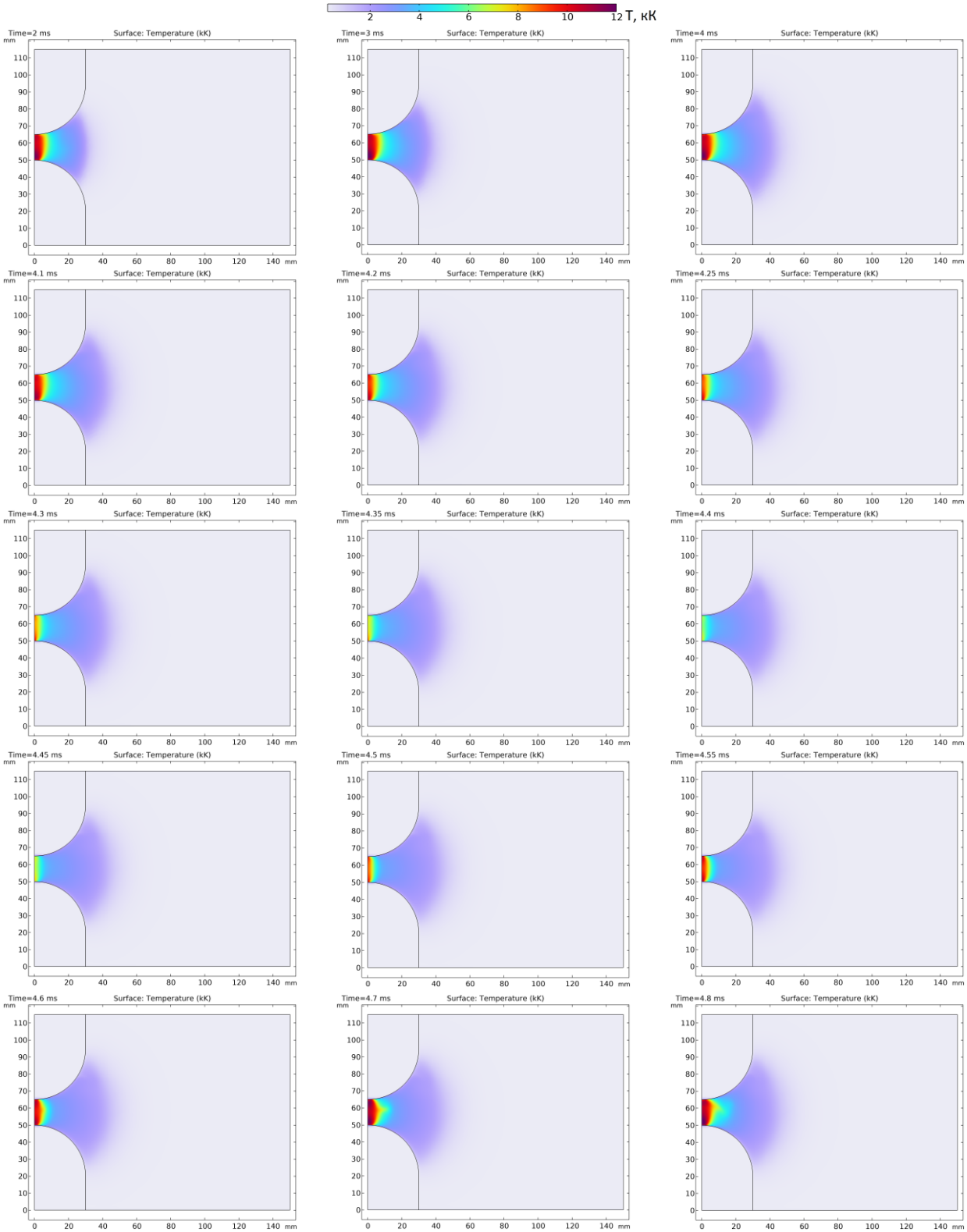

Figure 11. Distribution of arc plasma temperature at different time moments for the case without arc extinction, charging voltage $U_{ch,4}$ = 900 V (Case 4) for the following moments of time (in ms): 2; 3; 4; 4.1; 4.2; 4.25; 4.3; 4.35; 4.4; 4.45; 4.5; 4.55; 4.6; 4.7; 4.8 (the time interval of 0–2 ms is not shown, as the temperature distributions do not differ from the previously presented results for Case 2, see Figure 8)

The obtained time-dependent characteristics of the arc current and arc voltage allow to determine the arc quenching criterion described in (30, 31).

Based on Slepian's similarity law, which relates to the recovery of the electrical strength of the interelectrode gap under arc quenching conditions, the following equation is used:

$$Q_0 \frac{dR_{arc}}{R_{arc}dt} = U_{arc} \cdot I_{arc} - P_{loss}. \quad (4)$$

The left-hand side of this equation is set to zero, i.e., the power supplied to the arc, $U_{arc} \cdot I_{arc}$, is equated to the arc power loss P_{loss} on the right-hand side.

During the burning of an electric arc, the arc voltage varies depending on the conditions affecting the arc column. Prior to current zero crossing (or before extinction), the arc voltage increases sharply, then decreases and crosses zero along with the arc current. The power delivered to the arc from the source, which must be compared to the arc power loss, can be calculated as the product of the maximum voltage value before the zero crossing and the value of the arc current at the same moment of time.

For the two calculated cases with arc quenching, the time instants at which the arc voltage reaches its maximum prior to extinction were determined. At these instants, the values of the arc voltage and the arc current were identified. The product of these quantities yields the minimum power required to sustain an electric arc in the given geometry. These data are presented in Table 2.

For comparison, Table 2 also presents the results for Cases 3 and 4. Since no quenching occurred in these cases, the time instant corresponding to the minimum current was used.

Table 2 shows that the minimum input power required to sustain the electric arc ranges from 14.5 to 17.5 kW for the given geometry. It follows that in Case 4, when the arc current decreased from 2390 A to 47 A and the input power to the arc dropped to 14.5 kW, the arc was in a critical state near extinction at that time instant (4.408 ms).

Due to the inability to conduct experimental studies in a high-current generator network (exceeding 200 kA), the feasibility of this short-circuit current-limiting method was evaluated theoretically.

TABLE 2. Determination of the electric arc quenching criterion

Case number	Moment in time t, ms	Voltage, V	Current, A	Power, kW
1	4.300	221	66	14.586
2	4.305	201	87	17.533
3*	4.600	159	434	69.006
4*	4.408	309	47	14.523

Note: *Since there was no quenching in these cases, the values are given for the time when the current was minimal.

For this purpose, a model of an AC generator network was performed in the MATLAB Simulink software, featuring two 800 MVA generators with a rated voltage of 24 kV (32). That model was used for calculating transient processes during a three-phase short circuit.

A capacitor bank (see Figure 12), with a capacitance of 7 mF and pre-charged to 24 kV, is switched to the network via thyristors and discharged, thereby generating a counter current through the generator circuit breaker.

The thyristor control system is designed such that the control signal is sent to thyristor groups (depending on current polarity) only after the current through the arc-quenching contacts reaches 160 kA.

The simulation results namely time-dependent phase currents for cases without and with current limitation are presented in Figure 13.

It can be observed that the maximum phase short-circuit currents for the case without the counter electromagnetic field action are $I_{A,max}$ = 177 kA, $I_{B,max}$ = 241 kA, $I_{C,max}$ = 190 kA (see Figure 13a).

And the maximum phase short-circuit currents are significantly reduced for the case with the application of the counter electromagnetic field: $I_{A,max}$ = 98 kA, $I_{B,max}$ = 171 kA, $I_{C,max}$ = 133 kA (see Figure 13, b). This reduction enables generator circuit breakers to successfully interrupt currents of such magnitudes.

4. CONCLUSION

The paper presents a novel principle for influencing high-current electric arcs using a counter electromagnetic field. The results of experimental studies and mathematical simulation of the processes under investigation, conducted on a model test bench, are presented. A comparison of these results showed close values, a discrepancy has the order of 5-10%.

Figure 12. Example of capacitor bank implementation

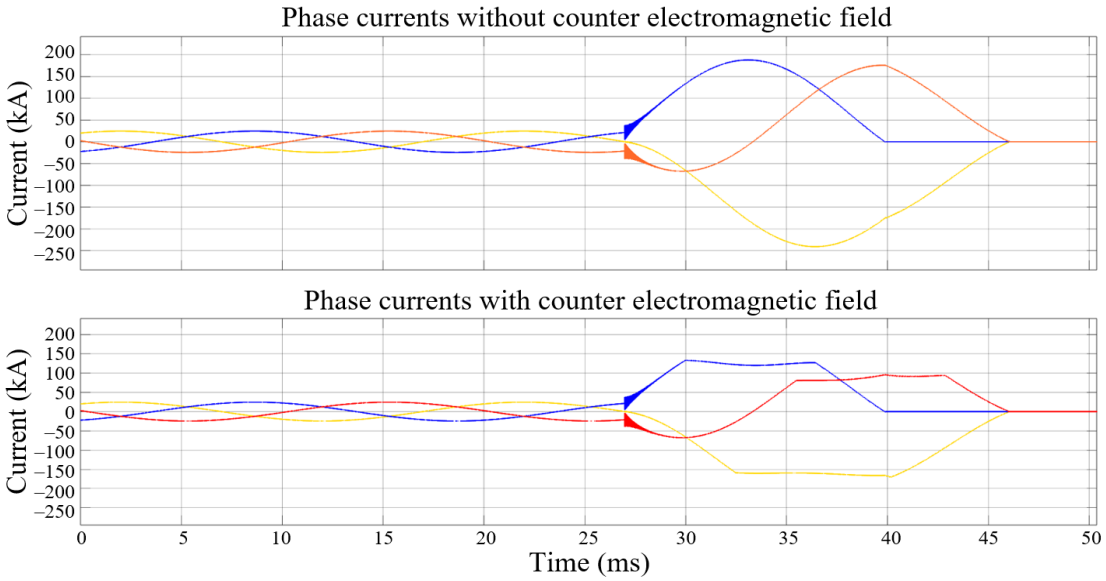

Figure 13. Time dependencies of the phase currents in the AC generator network model for the cases without and with current limitation, applied during the simulation of transients under a three-phase short-circuit condition

The duration of the arc quenching transient process depends on the switching circuit inductance, the time constant of the capacitor (circuit) discharge, and the properties of the arc discharge itself. These properties change based on the electron flux generated by the counter field, that phenomenon requires further investigation.

For a charging voltage of $U_{ch,1}$=500 V and main circuit capacitances of $C1$=11.4 mF and $C2$=0.78 mF, the maximum arc current prior to quenching was $I_{arc,max}$=1283 A, and the arc quenching time was t_{quench}=0.315 ms. For a charging voltage of $U_{ch,2}$=900 V and the same capacitance values, the maximum arc current was $I_{arc,max}$=2390 A, and the quenching time was t_{quench}=0.328 ms.

Thus, although the arc current increased by a factor of 1.86 (implying a significant increase in the energy stored in the arc), the quenching time remained virtually unchanged (a mere 4% variation).

This can be explained by the fact that the increased charging voltage also raises the energy stored in the counter-pulse capacitor $C2$, thereby enhancing the influence of the counter electromagnetic field on the arc. It follows that for the same arc current, increasing the energy of the counter electromagnetic field would lead to a reduction in the arc quenching time.

Furthermore, the minimum input power required to sustain an electric arc for the geometry under consideration was determined based on the similarity theory of D. Slepian concerning the recovery of dielectric strength in the gap and the conditions for arc quenching. This value was found to be in the range of 14.5–17.5 kW.

The feasibility of applying this current-limiting method to high-current generator circuits (exceeding 200 kA) was assessed theoretically. Calculations performed using the MATLAB Simulink software demonstrated that the application of the counter-pulse technique reduces the generator network current by a factor of 1.4–1.8, bringing it down to levels manageable by the circuit breaker.

In this way, applying the aforementioned short-circuit current-limiting method in high-current generator networks entails an increase in the physical dimensions of electrical equipment due to the inclusion of an additional cabinet (see Figure 12) but this approach resolves the issue of enhancing the switching resource of the generator circuit breaker.

The obtained data are particularly valuable for understanding the interaction effects between the arc discharge and the counter electromagnetic field quenching system. The results demonstrate the complex nonlinear dynamics of transient processes in high-energy circuits. The observed specific features of voltage variation during different phases of the process provide crucial information for the further improvement of arc suppression system parameters and the development of more accurate mathematical models of this physical phenomenon.

Acknowledgements

The authors appreciate Higher School of Electric Power Systems, Institute of Energy, Peter the Great St. Petersburg Polytechnic University for providing necessary facilities to conduct the present research.

Funding

The research was carried out within the state assignment of Ministry of Science and Higher Education of the Russian Federation (theme No. FSEG-2023-0012).

Ethics Approval and Consent to Participate

This article does not involve any studies with human participants or animals performed by any of the authors. Therefore, ethics approval and consent to participate are not applicable.

Competing Interests

The authors declare no financial or organizational conflicts of interest.

Data Availability

The data that support the findings of this study are available upon reasonable request.

Declaration of Generative AI and AI-assisted Technologies in the Writing Process

During the preparation of this manuscript, the authors used Deepseek exclusively for minor language editing to improve readability. After using this tool, the author carefully reviewed and edited the content as needed and takes full responsibility for the content of the published article.

Authors Biosketches

V. Y. Frolov – Dr. Sci. (Eng.), Professor. A scientist specializing in research and modeling of processes in switching devices of electrical apparatus, plasma technologies and electrical engineering systems.
V. V. Barskov – Dr. Sci. (Eng.), Docent. A scientist specializing in research and modeling of thermal energy processes and and electrical engineering systems.
D. V. Ivanov – Cand. Sci. (Eng.), Docent. Research interests are in the field of research and modeling of electrical engineering and electro thermal processes.
A. Sabbaghan – PhD Student. Research interests are in the field of research and modeling of switching devices of electrical apparatus and electrical engineering processes.

REFERENCES

1. Sattarpour T, Nazarpour D. Assessing the impact of size and site of distributed generations and smart meters in active distribution networks for energy losses cost. International Journal of Engineering Transactions A: Basics. 2015;28(7):1002-10. https://doi.org/10.5829/idosi.ije.2015.28.07a.06
2. Sedighi AR, Hamidian MJ. A novel method for implementing of time-of-use to improve the performance of electric distribution systems: a case study. International Journal of Engineering Transactions C: Aspects. 2017;30(3):357-65. https://doi.org/10.5829/idosi.ije.2017.30.03c.05
3. Hosseini Mola J, Barforoshi T, Adabi Firouzjaee J. Distributed generation expansion planning considering load growth uncertainty: a novel multi-period stochastic model. International Journal of Engineering Transactions C: Aspects. 2018;31(3):405-14. https://doi.org/10.5829/ije.2018.31.03c.02
4. Abbasghorbani M. Prioritization of transmission network components based on their failure impact on reliability of composite power systems. International Journal of Engineering Transactions C: Aspects. 2022;35(3):502-9. https://doi.org/10.5829/IJE.2022.35.03C.0
5. Rezaei M, Tolou-Askari M, Amirahmadi M, Ghods V. Challenges of generation and transmission expansion planning considering power system resilience and provide solutions. International Journal of Engineering Transactions B: Applications. 2023;36(5):824-41. https://doi.org/10.5829/IJE.2023.36.05B.01
6. Maintenance of GIS type ELK SF6 gas-insulated switchgear. Technical information ABB HASV 685 350 E – AK 35.0 – B 10/96
7. Hermosillo V, Leguizamon-Cabra D, Catala M, Darles L, Gregoire C, Rodriguez J. Comparative continuous and overload current performance of high voltage switchgear with SF6 and alternative gases. CIGRE Session, Ref A3-10126_2022. Paris, France; 2022. https://www.e-cigre.org/publications/detail/a3-10126-2022-comparative-continuous-and-overload-current-performance-of-high-voltage-switchgear-with-sf6-and-alternative-gases.html
8. Simka P, Seeger M, Votteler T, Schwinne M. Experimental investigation of the dielectric strength of hot SF6. IEEE 10th International Conference on the Properties and Applications of Dielectric Materials. 2012;IEEE. https://doi.org/10.1109/ICPADM.2012.6319001
9. Varetsky Y, Gajdzica M. Study of short circuit and inrush current impact on the current-limiting reactor operation in an industrial grid. Energies. 2023;16(2):811. https://doi.org/10.3390/en16020811
10. Ouaida R, de Palma JF, Gonthier G. DC GRIDS: new over current protection. 18th European Conference on Power Electronics and Applications (EPE'16 ECCE Europe). 2016;IEEE. https://doi.org/10.1109/EPE.2016.7695335
11. Doljack F. PolySwitch PTC devices – a new low-resistance conductive polymer-based PTC device for overcurrent protection. IEEE Transactions on Components, Hybrids, and Manufacturing Technology. 1981;4(4):372-8. https://doi.org/10.1109/TCHMT.1981.1135838
12. Bell JG, Graule T, Stuer M. Barium titanate-based thermistors: past achievements, state of the art, and future perspectives. Applied Physics Reviews. 2021;8(3):031318. https://doi.org/10.1063/5.0048697
13. Safonov E, Frolov V, Zhiligotov R, Petrenya Yu. The specifics of PTC thermistor applications for limiting surge currents. Energies. 2024;17(2):318. https://doi.org/10.3390/en17020318
14. Frolov VYa, Shidlovskiy DV, Safonov EP. Development of diode based synchronous load break switch. 2022 Conference of Russian Young Researchers in Electrical and Electronic Engineering (ElConRus). 2022;IEEE. https://doi.org/10.1109/ElConRus54750.2022.9755470
15. Magnus C, Blomberg A, Häfner F, Jacobson B. The hybrid HVDC breaker. ABB Grid Systems, Technical Paper Nov 2012.

https://www.ingegneriaelettrica.net/documenti/ABB_hybrid-hvdc-breaker.pdf

16. Safonov E, Frolov V, Zhiligotov R, Petrenya Yu. On the problems of current limitations in networks based on power semiconductor devices. Energies. 2023;16(16):5905. https://doi.org/10.3390/en16165905
17. Safonov EP, Frolov VYa, Boeshko AV, Dautov RS. A semiconductor current-limiting device based on a DC converter. Energies. 2025;18(1):58. https://doi.org/10.3390/en18010058
18. Mogilevsky GV. Gibridnye ehlektricheskie apparaty nizkogo napryazheniya (Low-voltage hybrid electrical devices). Moscow: Russia. Energoatomizdat; 1986
19. Kukekov GA, Frolov VYa. Perekhodnye process v kontaktno-tiristornyh apparatah (Transient processes in contact-thyristor apparatuses). Leningrad: Russia. Energoatomizdat; 1988
20. Soskov AG, Soskova IA. Poluprovodnikovye apparaty: kommutaciya, upravlenie, zashchita (Semiconductor apparatuses: switching, control, protection). Kyiv: Ukraine. Karavella; 2005
21. Naidu IES, Padmavathi T, Padmavathi SV, Kumar BU. Intelligence based controlling models for effective power tracking and voltage enhancement in Grid-PV systems. Emerging Science Journal. 2025;9(1):261-83. https://doi.org/10.28991/ESJ-2025-09-01-015
22. Baghdasaryan M, Hovhannisyn V. Stability assessment of an ore mill electric drive using machine learning. HighTech and Innovation Journal. 2024;5(2):213-30. https://doi.org/10.28991/HIJ-2024-05-02-01
23. Meyer Ch, De Doncker R, Kowal M. Current-limiting switch. WO Patent WO 2007/022744. 25 August 2005
24. Wei X, Gao C, He Z, Zhang S. Passive high-voltage direct-current circuit breaker and implementation method therefor. EP Patent 3,131,166. 30 December 2014
25. Guo Q. Direct-current arc-extinguishing circuit and device. EP Patent 3648133. 24 July 2017
26. Frolov VYa, Ivanov VN, Ivanov DV. Mathematical models of plasma electrotechnological processes. Electricity. 2018;7:54-60. https://doi.org/10.24160/0013-5380-2018-7-54-60
27. Dresvin SV, Ivanov DV. Fizika plazmy (Plasma Physics). St. Petersburg: Russia. Polytechnic University Publishing House; 2013
28. Mürmann M, Chusov A, Fuchs R, Nefedov A, Nordborg H. Modeling and simulation of the current quenching behavior of a line lightning protection device. Journal of Physics D: Applied Physics. 2017;50(10):105203. https://doi.org/10.1088/1361-6463/aa560e
29. Frolov VYa, Ivanov DV, Sivaev AD, Chusov AN, Chistyakov AS, Rogozhina AA. Mathematical model of arc extinguishing in adjacent chambers of the RMKE-10 lightning protection multi-chamber arrester. Electricity. 2022;7:40-51. https://doi.org/10.24160/0013-5380-2022-7-40-51
30. Petrenya YuK, Frolov VYa, Ivanov DV. Fiziko-tekhnicheskie aspekty dissipacii ehnergii dugovoj plazmy. Tom 1 (Physical and technical aspects of arc plasma energy dissipation. Volume 1). St. Petersburg: Russia. POLYTECH-PRESS; 2023
31. Satchilembe VL, Frolov VYa, Ivanov DV. Condition of electric arc quenching in an arc extinguishing device. 23rd International Symposium on Electrical Apparatus and Technologies (SIELA 2024). 2024;IEEE. https://doi.org/10.1109/SIELA61056.2024.10637830
32. Frolov VYa, Podporkin GV, Ivanov DV. Fiziko-tekhnicheskie aspekty dissipacii ehnergii dugovoj plazmy. Tom 2 (Physical and technical aspects of arc plasma energy dissipation. Volume 2). St. Petersburg: Russia. POLYTECH-PRESS; 2025

Persian Abstract

چکیده

بر اساس تحلیل منابع قطع در کلیدهای مدارشکن ژنراتور، به دلیل عدم امکان افزایش ظرفیت قطع تجهیزات الکتریکی با روش‌های سنتی، نیاز به محدودسازی جریان مشخص شد. پس از ارائه تحلیلی از روش‌های موجود محدودسازی جریان، یک اصل جدید برای اثرگذاری بر قوس الکتریکی پرجریان توسط میدان الکترومغناطیسی متقابل پیشنهاد گردید. نتایج مطالعات تجربی و شبیه‌سازی ریاضی فرآیندهای مورد نظر ارائه شده است؛ مقایسه این نتایج نشان‌دهنده توافق خوبی است که اعتبارسنجی موفقیت‌آمیز مدل توسعه‌یافته را تأیید می‌کند.راه‌حل‌های فنی برای کنترل محدودسازی‌های جریان توسعه یافته است. در این راستا، اصل تأثیر الکترومغناطیسی بر قوس به تفصیل بررسی شده و پارامترها و ویژگی‌های کنترلی آن تعیین گردیده است.